Supplementary Materials:

Unprecedented robust antiferromagnetism in fluorinated hexagonal perovskite

Mihai Sturza[1], Houria Kabbour[1], Sylvie Daviero-Minaud[1], Dmitry Filimonov[2], Konstantin Pokholok[2], Nicolas Tiercelin[3], Florence Porcher[4], Laurent Aldon[5], Olivier Mentré[1,*]

[1] *Université Lille Nord de France. UCCS, CNRS UMR 8181, ENSCL-USTL, Villeneuve d'Ascq, France.*

[2]*Department of Chemistry, Moscow State University, 119991 Moscow, Russia*

[3] *International Associated Laboratory LEMAC: IEMN, UMR CNRS 8520, PRES Lille Nord de France, EC Lille, Villeneuve d'Ascq, France*

[4]*Laboratoire Léon Brillouin, CEA Saclay, 91191 Gif-sur-Yvette Cedex, France*

[5] *Université Montpellier 2, CNRS, Inst. Ch. Gerhardt, UMR 5253, France*

*E-mail: olivier.mentre@ensc-lille.fr

S1. Computation methods

DFT calculations methods: Density functional theory (DFT) calculations were performed using the Vienna *ab* initio simulation package.[1] The calculations were carried out within the generalized gradient approximation (GGA) for the electron exchange and correlation corrections using the Perdew-Wang[2] functional and the frozen core projected wave vector method.[3] The full geometry optimizations were carried out using a plane wave energy cutoff of 550 eV and 42 or 50 *k* points (depending on the structural model) in the irreducible Brillouin zone. All structural optimizations converged with residual Hellman-Feynman forces on the atoms smaller than 0.03 eV/Å. The geometry optimizations were performed using non-spin-polarized calculations so that no magnetic configuration is favored. The structural models 6H-$BaFeO_3$, 6H-$BaFeO_{2.66}F_{0.33}$ and 6H-$BaFeO_{2.33}F_{0.33}$ were built from the initial structure of 6H-$BaFeO_3$ and then fully relaxed as described above (fig. S1b).

For the total energies calculations, GGA plus on-site repulsion (GGA+U)[4] calculations were employed to account for the strong electron correlation associated with the 3d electrons on the Fe atoms. A plane wave energy cutoff of 400 eV, a total energy convergence threshold of 10^{-6} and 91 or 98 *k* points (depending on the structural model) in the irreducible Brillouin zone were used.

Table S1a. Relative energies of the different magnetic configurations used to extract the magnetic exchange parameters, for the three structural models for U_{eff}= 5 eV. The most stable configurations are set to 0.

		6H-$BaFeO_3$	6H-$BaFeO_{2.66}F_{0.33}$	6H-$BaFeO_{2.33}F_{0.33}$
Relative energies (eV/unit cell)	FM	0	0.18601	2.01973
	AF1	0.96249	0	0
	AF2	1.01926	0.12871	0.53268

In order to access the J values, the total energies of the three ordered spin states FM, AF1 and AF2 depicted in **Fig. S1d** were calculated using GGA+U calculations with U_{eff}= 5eV, increasing the U_{eff} value up to 6 eV led to qualitatively the same results. Their relative energies are summarized in **Table S1a** for the three models, namely 6H-$BaFeO_3$, 6H-$BaFeO_{2.66}F_{0.33}$ and 6H-$BaFeO_{2.33}F_{0.33}$. In the case of 6H-$BaFeO_3$, the most stable state is found to be ferromagnetic, while for 6H-$BaFe_{2.66}F_{0.33}$ and 6H-$BaFe_{2.33}F_{0.33}$, the anti-ferromagnetic AF1 configuration is found to be the most stable.

The 6H-$BaFeO_3$ has been barely studied from the theoretical point of view [5]. However, many experimental studies were carried out for compounds 6H-$BaFeO_{3-\delta}$ exhibiting slight oxygen deficiency. AFM ordering and semiconducting behavior has been reported in most cases. Evidence of charge disproportionation has been reported in several articles, by means of Mossbauer studies in particular. The charge disproportionation is announced to accompany both a magnetic transition and a charge ordering without major structural changes [6-9]. In our calculations of the structural model 6H-$BaFeO_3$, an ideal structure is taken in account so that the expected average oxidation state for iron is Fe^{4+}. The observed complex behavior complicates proper electronic structure calculations on these oxides as well as on the fluorinated compounds. As a matter of fact, difficulties were encountered for some of the configurations. Nevertheless, accurate total energies could be obtained and were used to extract the J values (see below).

The energies of the ordered spin states are expressed using the spin Hamiltonian,

$$\hat{H} = -\sum_{i<j} J_{ij}\, \hat{S}_i \cdot \hat{S}_j$$

where J_{ij}= (J1, J2) correspond to the SE parameters for the spin site i and j. The total SE energies are written as follows:

$$E_{FM} = (-12J1 - 2J2)N^2/4$$
$$E_{AF1} = (12J1 - 2J2)N^2/4$$

$$E_{AF2} = (12J1 + 2J2)N^2/4 \text{ (exp)}$$

The magnetic exchange parameters J1 and J2 are then extracted by equating relative energies of the different magnetic configurations to the corresponding energy differences from the total SE energies. J1 and J2 are reported in **Table 2** for each of the studied structural model.

References

1. Kresse G.; Furthmüller J. Vienna Ab-initio Simulation Package (VASP); Institut für Materialphysik: Vienna, **2004**; http://cms.mpi.univie.ac.at/vasp.
2. Kresse, G.; Joubert, D. *Phys. Rev. B* **1999**, *59*, 1758.
3. Perdew, J. P.; Wang, Y. *Phys. Rev. B* **1992**, 45, 13244.
4. Dudarev, S. L.; Botton, G. A.; Savrasov, S. Y.; Humphreys, C. J.; Sutton, A. P. *Phys. Rev. B* **1998**, *57*, 1505.
5. Hong-Jian, F.; Fa-Min, L., *Chinese Physics B*, **2008**, *17*, 1874.
6. Mori, K.; Kamiyama, T.; Kobayashi, H.; Oikawa, K.; Otomo, T.; Ikeda, S. *Phys. Soc. Jpn.* **2003**, *72*, 2024–2028.
7. Morimoto, S.; Kuzushita, K.; Nasu S. *J. Magn. Magn. Mater.*, **2004**, *272-276*, 127.
8. Mori, K.; Kamiyama, T.; Kobayashi, H.; Itoh, K.; Otomo, T.; Ikeda, S. *Physica B*, **2003**, *329-333*, 807.
9. Gil de Muro, I.; Insausti, M. ; Lezama, L. ; Rojo, T. *J. Solid State Chem.*, **2005**, *178*, 1712.

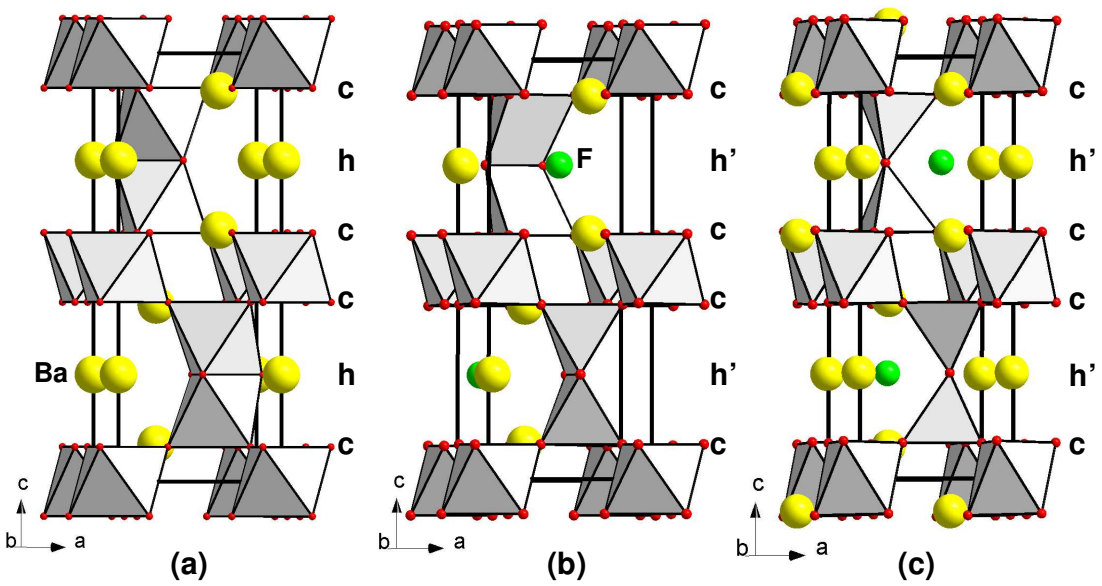

Figure S1b. *Structural model after optimization of (a) 6H-$BaFeO_3$, (b) 6H-$BaFeO_{2.66}F_{0.33}$ and (c) 6H-$BaFeO_{2.33}F_{0.33}$*

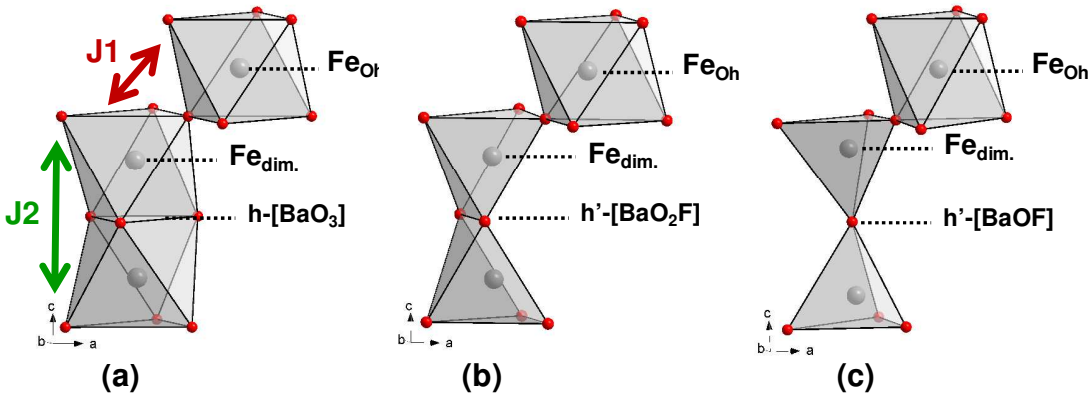

Figure S1c. *Local environments in (a) 6H-$BaFeO_3$: a face-sharing octahedrons dimmer linked by the outer corners to octahedrons. J1 is indicated as a red arrow and represent the magnetic interaction Fe_{oh}-Fe_{dim}. Fe_{dim} refers to iron atoms within the dimmers and Fe_{oh} to iron atoms within corner sharing only octahedrons. J2 is indicated as a green arrow and refers to the intra-dimmer magnetic interaction Fe_{dim}-Fe_{dim}. (b) 6H-$BaFeO_{2.66}F_{0.33}$: here the dimmers are formed by edge-sharing pyramids and are linked to octahedrons by the outer corners. And (c) 6H-$BaFeO_{2.33}F_{0.33}$: here the dimmers are formed by corner-sharing tetrahedrons linked to octahedrons through their outer corners. Fe_{oh}, Fe_{dim}, J1 and J2 are only indicated in (a) but do also apply in the case of (b) and (c).*

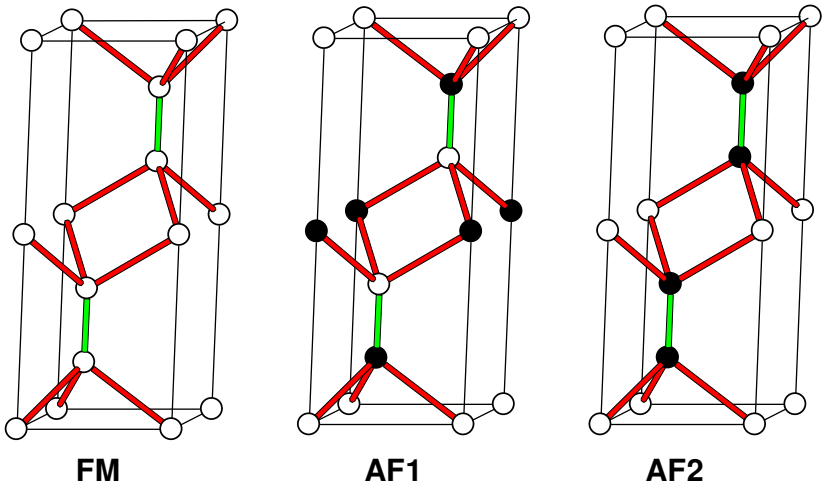

Figure S1d. *Representation of the three magnetic configurations used in our calculations: FM, AF1 and AF2. Only Fe atoms are represented for clarity. Up spins are represented by empty circles and down spins by black filled circles. J1 and J2 are indicated by red and green bonds between Fe atoms, respectively.*

S2. Room-temperature Neutron Diffraction for 6H-$Ba_{0.8}Sr_{0.2}FeF_{0.2}O_{3-\delta}$ and 15R-$BaFe^{+3.04}F_{0.2}O_{2.42}$

The structure is disordered, with a mixing of several iron coordinations in the hexagonal slabs. It creates a variety of Ba and Fe local coordinates, which are evidenced by the splitting and/or strong thermal anisotropy of atoms along the c-axis. The difficulty during

the refinement arises from this disordered assorted with antiferromagnetic ordering even at room temperature.

Table S2a: Atomic parameters from the powder Neutron experiment for $Ba_{0.8}Sr_{0.2}Fe^{+3.16}F_{0.2}O_{2.48}$ (a = 5.70493(5) Å, c = 14.2735(2) Å, Bragg R-factor: 5.86%; Rf-factor= 5.88%). Atomic coordinates and isotropic thermal displacement parameters.

Atom	Wyck. /Occ.	x	Y	z	U eq./iso* ($Å^2$)
Ba1	2b/1.00(4)	0	0	1/4	0.0166(4)
Sr1	2b/0.42(4)	0	0	1/4	0.0166(4)
Ba2	4f/1.20(2)	1/3	2/3	0.0804(3)	0.0166(4)
Sr2	4f/0.22(2)	1/3	2/3	0.0804(3)	0.0166(4)
Fe1	2a/1.4169	0	0	0	0.0091(3)
Fe2	4f/0.70(3)	1/3	2/3	0.8731(7)	0.0091(3)
Fe2'	4f/0.75(3)	2/3	1/3	0.1541(7)	0.0091(3)
O1	12k/1.4169	0.8355(5)	0.6711(5)	0.08538(12)	0.0258(3)
hexagonal layer : anions					
$(O,F)_{Oh}$	6h/(0.592(9))	0.5296(13)	0.0591(13)	1/4	0.0258(3)
O_{Td}	6h/0.161(8)	0.615(4)	0.229(4)	1/4	0.0258(3)
F_{Ba5}	6h/0.213(7)	0.381(3)	0.762(3)	1/4	0.0258(3)

The deduced distribution of $Fe_2(O,F)_{9-x}$ polyhedra in the hexagonal slabs :

$Fe_2(O,F)_9$ octahedral face-shared dimers = few% ;
$Fe_2(O,F)_8$ penta-coordinated edge-shared dimers = 56%
Fe_2O_7 tetrahedral dimers = 34%

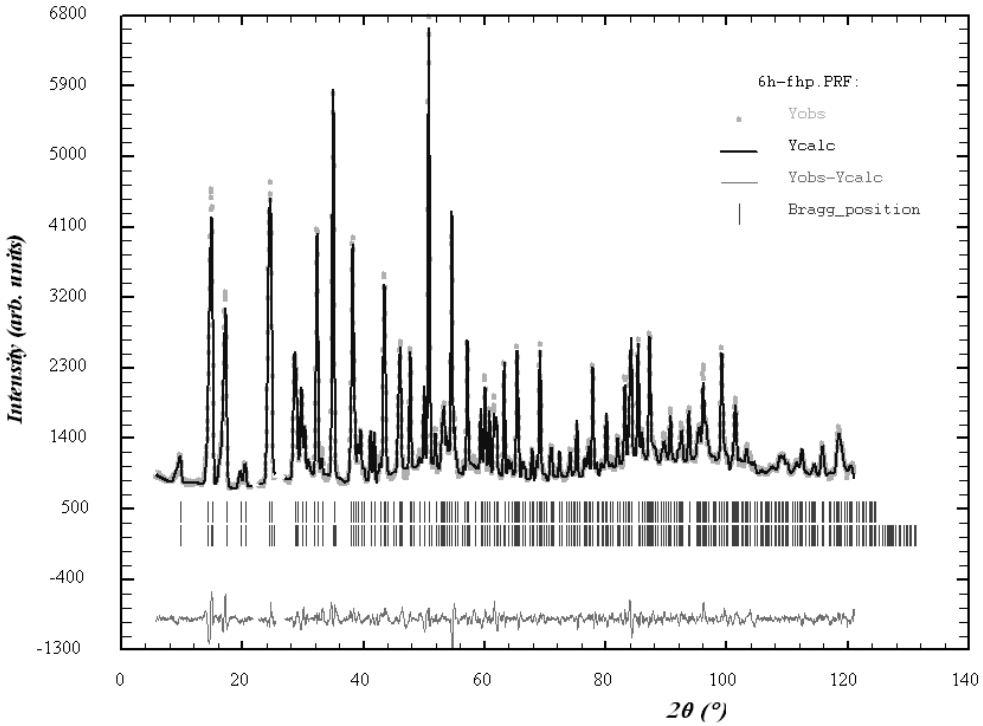

Figure S2b: *Calculated and observed ND-profiles of the Rietveld refinement for $Ba_{0.8}Sr_{0.2}Fe^{+3.16}F_{0.2}O_{2.48}$, 3T2 difractometer ($\lambda$ = 1.2254 Å, Bragg R-factor: 5.86%; Rf-factor= 5.88%; R-mag=5.67%). The second phase corresponds to the antiferromagnetic magnetic structure which exists at room-temperature*

Table S2c: Selected bond distances (Å) in $Ba_{0.8}Sr_{0.2}Fe^{+3.16}F_{0.2}O_{2.48}$. The distances noted* are too short, due to the bad localization of Fe2 and Fe2' in their tetrahedral coordination, masked by their thermal vibration along c.

atoms	**d(Å)**
Fe1 – O1(x6)	**2.031(2)**
$Fe2'_{Oh}$ – O1(x3)	**1.936(6)**
$Fe2'_{Oh}$ – $(O,F)_{Oh}$(x2 or x3)	**1.926(8)**
$Fe2'_{Td}$ – O1(x3)	**1.936(6)**
$Fe2'_{Td}$ – O_{Td} (x1)	**> 1.463(2)***
$Fe2_{Oh}$ – O1 (x3)	**1.771(4)**
$Fe2_{Oh}$ – $(O,F)_{Oh}$ (x2 or x3)	**2.219(9)**
$Fe2_{Td}$ – O1 (x3)	**1.771(4)**
$Fe2_{Td}$ – O_{Td}	**>1.831(1)***
Fe2' – Fe2'	**2.737(4)**
Fe2 – Fe2	**3.514(5)**
Fe2' – Fe2	**3.126(2)**
F_{Ba5} – Ba1(x3)	**3.085(2)- 3.765(1)**
F_{Ba5} – Ba2	**2.466(5)**

Table S2d: Atomic parameters from the powder Neutron experiment for *as-prepared* $BaFe^{+3.04}F_{0.2}O_{2.42}$ (a = 5.74912(9)Å, c = 36.1902(7)Å, Bragg R-factor: 8.28% ; Rf-factor= 7.33%). Atomic coordinates and isotropic thermal displacement parameters.

Atom	Wyck. /Occ.	x	y	z	U eq./iso. ($Å^2$)
Ba1	6c/1	0	0	0.1324(2)	0.022(3)
Ba2	6c/1	1/3	2/3	0.07043(20)	0.0152(12)
Ba3	3a/0.354(4)	0	0	0	0.005(2
Ba3'	6c/0.322(8)	0	0	0.0138(5)	0.005(2)
Fe1	3b/1	1/3	2/3	1/6	0.0112(9)
Fe2	6c/1	2/3	1/3	0.02458	0.0100(13)
Fe3	6c/1	2/3	1/3	0.10901	0.0214(10)
O1	9e/1	0	1/2	0	0.0213(8)
O2	18h/1	0.1682(4)	-0.1682(4)	0.20028(9)	0.0167(6)
hexagonal layer : anions					
$(O,F)_{Oh}$	18h/(0.39,0.07)	-0.1932(9)	0.1932(9)	0.0677(2)	0.043(3)
O_{Td}	18h/0.132(8)	-0.281(3)	0.281(3)	0.0688(9)	0.043(3)
F_{Ba5}	18h/0.096(5)	0.030(4)	-0.030(4)	0.0668(9)	0.043(3)

Table S2e: anisotropic thermal displacement parameters for $BaFe^{+3.04}F_{0.2}O_{2.42}$

Atom	U11	U22	U33	U12	U13	U23
Ba1	0.0042(8)	0.0042(8)	0.057(6)	-0.0021(8)	0.00000	0.00000
Fe2	0.0037(11)	0.0037(11)	0.0226(18)	-0.0062(11)	0.00000	0.00000
Fe3	0.00437(12)	0.00437(12)	0.055(3)	-0.00218(12)	0.00000	0.00000

The Deduced distribution of $Fe_2(O,F)_{9-x}$ polyhedra in the hexagonal slabs is :
$Fe_2(O,F)_9$ octahedral face-shared dimers = few% ;
$Fe_2(O,F)_8$ penta-coordinated edge-shared dimers = 71%
Fe_2O_7 tetrahedral dimers = 29%

Table S2f: Selected bond distances (Å) in $BaFe^{+3.04}F_{0.2}O_{2.42}$. The distances noted* are too short, due to the bad localization of Fe2 and Fe3 in their tetrahedral coordination, masked by their thermal vibration along c.

atoms	**d(Å)**
Fe1 – O2(x6)	**2.045(3)**
$Fe2_{Oh}$ – O1(x3)	**1.882(9)**
$Fe2_{Oh}$ – $(O,F)_{Oh}$(x2 or x3)	**2.093(6)**
$Fe2_{Td}$ – O1(x3)	**1.882(9)**
$Fe2_{Td}$ – O_{Td} (x1)	**>1.68(3)***
$Fe3_{Oh}$ – O2 (x3)	**1.887(2)**
$Fe3_{Oh}$– $(O,F)_{Oh}$ (x2 or x3)	**2.045(6)**
$Fe3_{Td}$– O2 (x3)	**1.887(2)**
$Fe3_{Td}$ – O_{Td} (x1)	**>1.55(3)***
Fe2 – Fe3	**3.055(5)**
F_{Td} – Ba2(x3)	**3.020(3)-3.483(1)**
F_{Td} – Ba1	**2.39(3)**
F_{Td} – Ba3'	**2.93(4)**

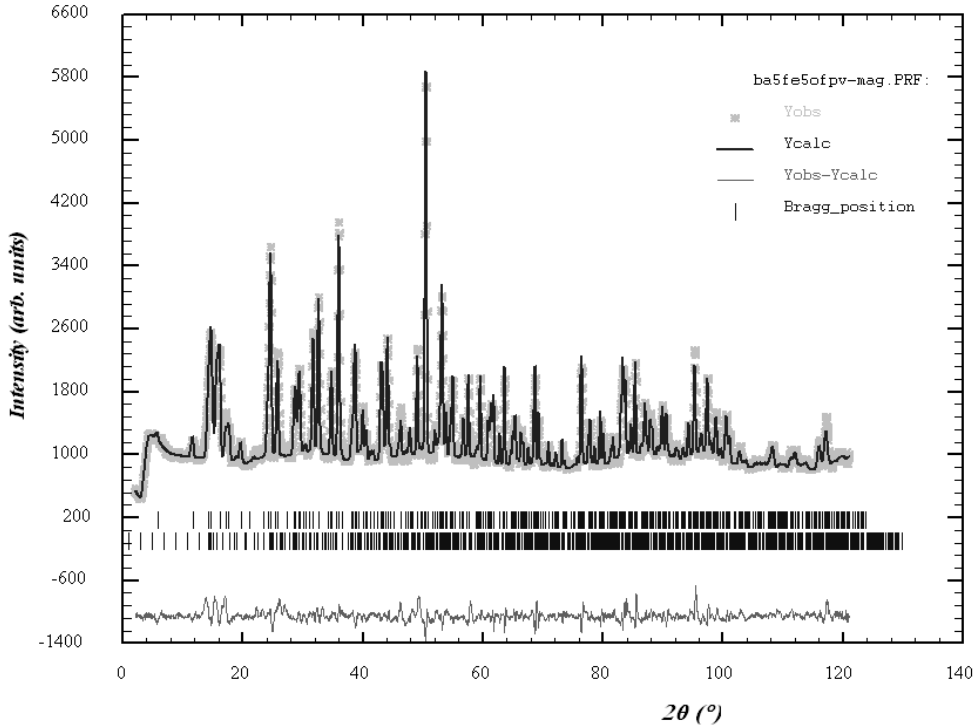

Figure S2g: *Calculated and observed ND-profiles of the Rietveld refinement for* $BaFe^{+3.04}F_{0.2}O_{2.42}$, *data collected with 3T2 difractometer (λ = 1.2254 Å, Bragg R-factor: 8.28% ; Rf-factor= 7.33%; R-mag=13.8%). The second phase corresponds to the antiferromagnetic magnetic structure which exists at room-temperature.*

S3. Low temperature powder neutron diffraction in the 15R-$BaFeF_{0.2}O_{3-x}$ (two samples : varying the volume $_{sample}$/volume $_{tube}$ ratio)

Several *as-prepared* 15R samples corresponding to x=0.2, have been obtained with various filling of the gold tube (modification of V_{powder}/V_{air}) before heating, have been investigated by means of neutron diffraction at room temperature. As a general result, the lattice parameters appear to depend on the synthesis conditions. For instance, a change of the c axis from 36.09 to 36.19 occurs on increasing $V_{powder}/V_{air.}$ Our structural refinements show that increasing the V_{powder}/V_{air} ratio (in favour of iron reduction) is accompanied by a lattice expansion. In fact this effect is very sensitive since by comparison between the compound $BaFe^{+3.04}F_{0.2}O_{2.42}$ prepared in a 3/4 filled gold tube (a = 5.74912(9)Å, c = 36.1902(7)Å) and $BaFe^{+3.08}F_{0.2}O_{2.44}$ prepared in a 2/3 filled gold tube (a = 5.74324(1)Å, c = 36.093(1)Å). The x=0.2 ratio is stoichiometrically conserved during the synthesis, on the basis of the F titration.

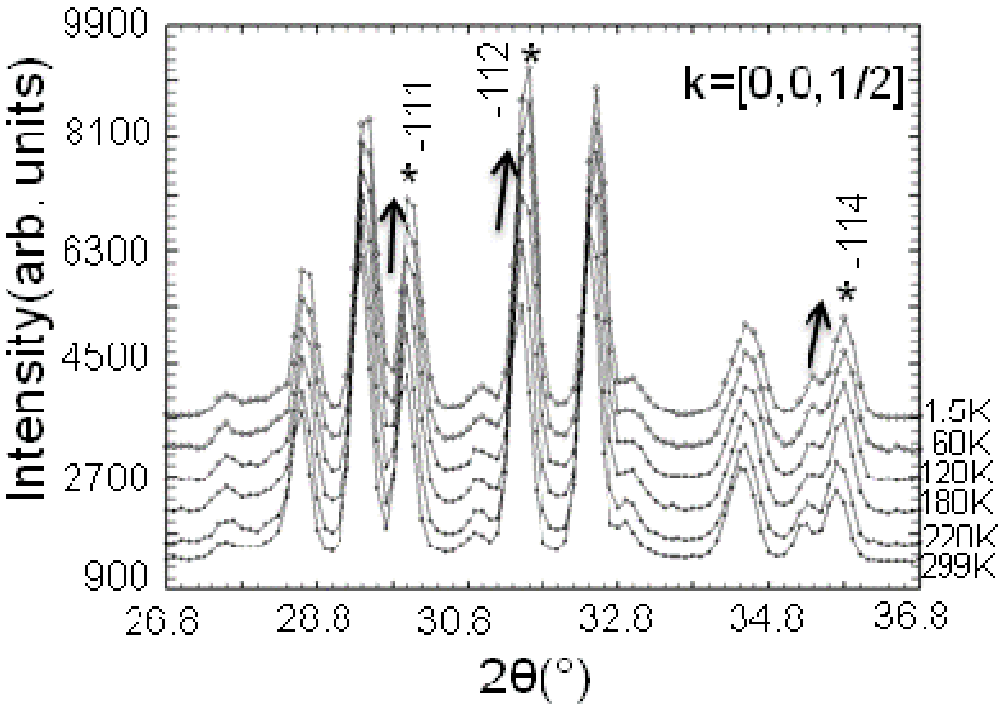

Figure S3a: *Variation of the magnetic peaks function of temperature for 15R-FHP* $BaFe^{+3.08}F_{0.2}O_{2.42}$*, data collected with the G41 diffractometer (λ=2.4226 Å).*

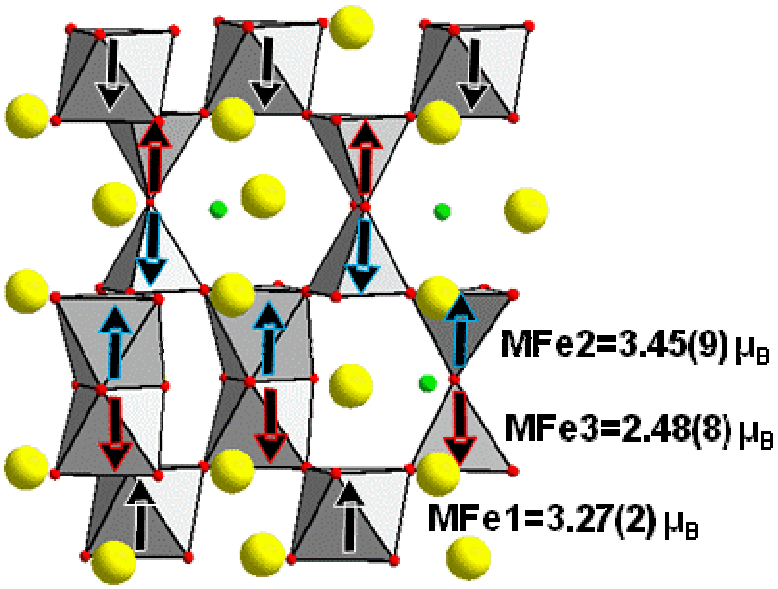

Figure S3b: *Magnetic structure for 15R-FHP* $BaFe^{+3.08}F_{0.2}O_{2.42}$ *at 299K data collected with the G41 diffractometer (λ=2.4226 Å, Bragg R-factor: 11.5%; Rf-factor= 13.2%; R-mag=18.9%).*

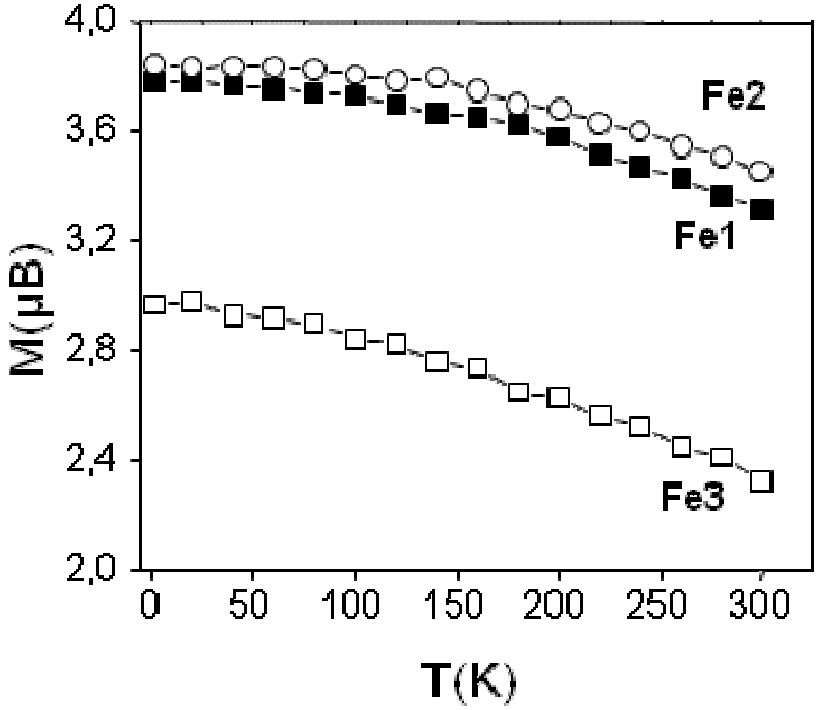

Figure S3c: *Variation of the refined magnetic moments for 15R-FHP $BaFe^{+3.08}F_{0.2}O_{2.42}$ as a function of temperature between 1.5K and 299K, data collected with the G41 diffractometer (λ=2.4226 Å).*

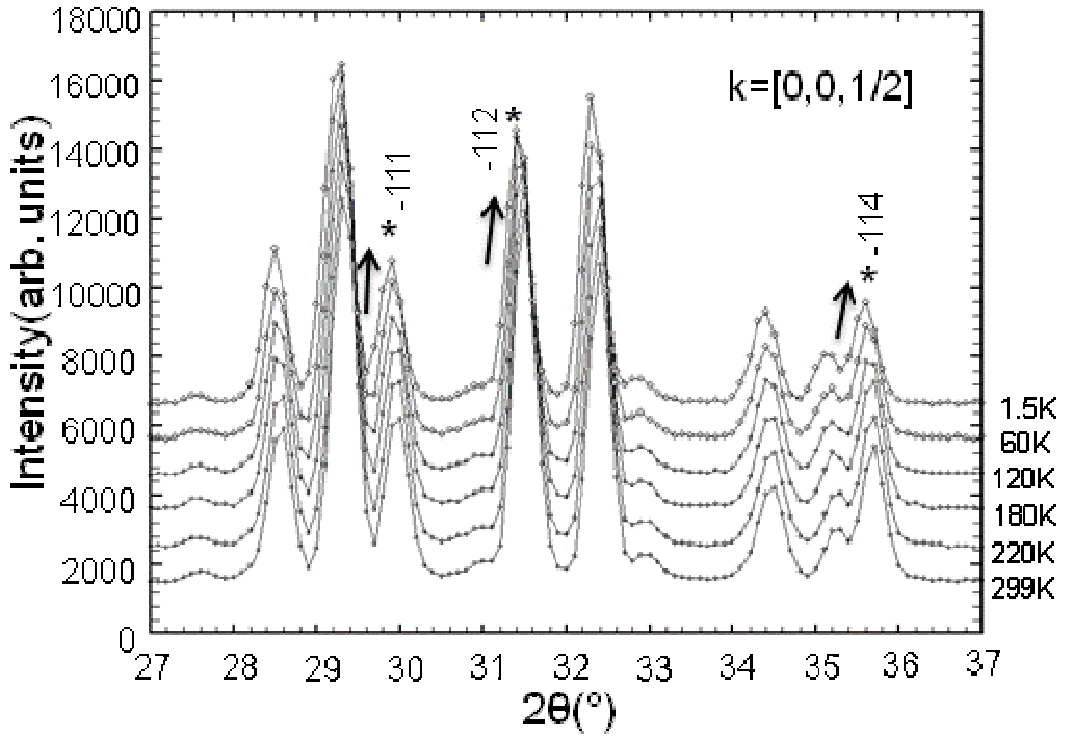

Figure S3d: *Variation of the magnetic peaks function of temperature for 15R-FHP $BaFe^{+3.04}F_{0.2}O_{2.42}$ data collected with the G41 diffractometer (λ=2.4226 Å).*

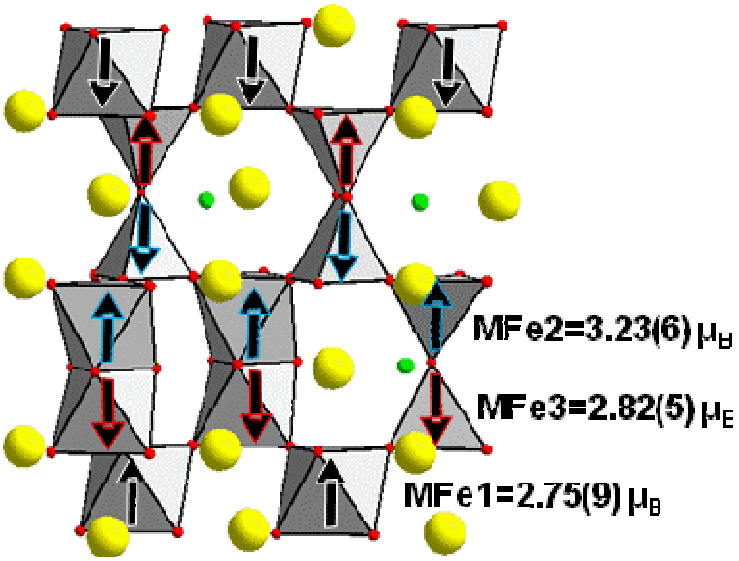

Figure S3e: *Magnetic structure for 15R-FHP $BaFe^{+3.04}F_{0.2}O_{2.42}$ at 299K data collected with the G41 diffractometer (λ=2.4226 Å, Bragg R-factor: 4.8%; Rf-factor= 2.49%; R-mag=4.54%).*

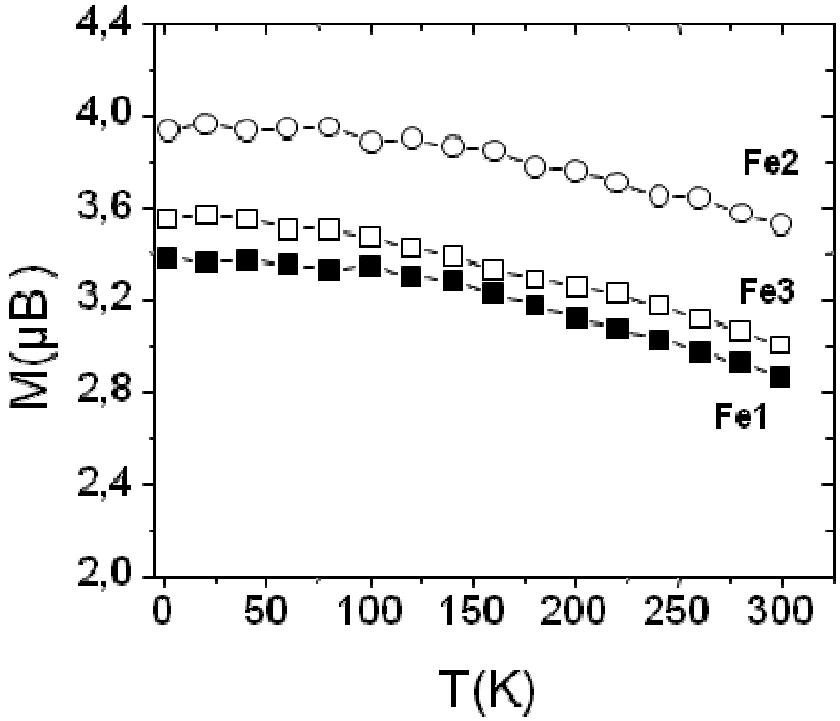

Figure S3f: *Variation of the refined magnetic moments for 15R-FHP $BaFe^{+3.04}F_{0.2}O_{2.42}$ as a function of temperature between 1.5K and 299K, data collected with the G41 diffractometer (λ=2.4226 Å).*

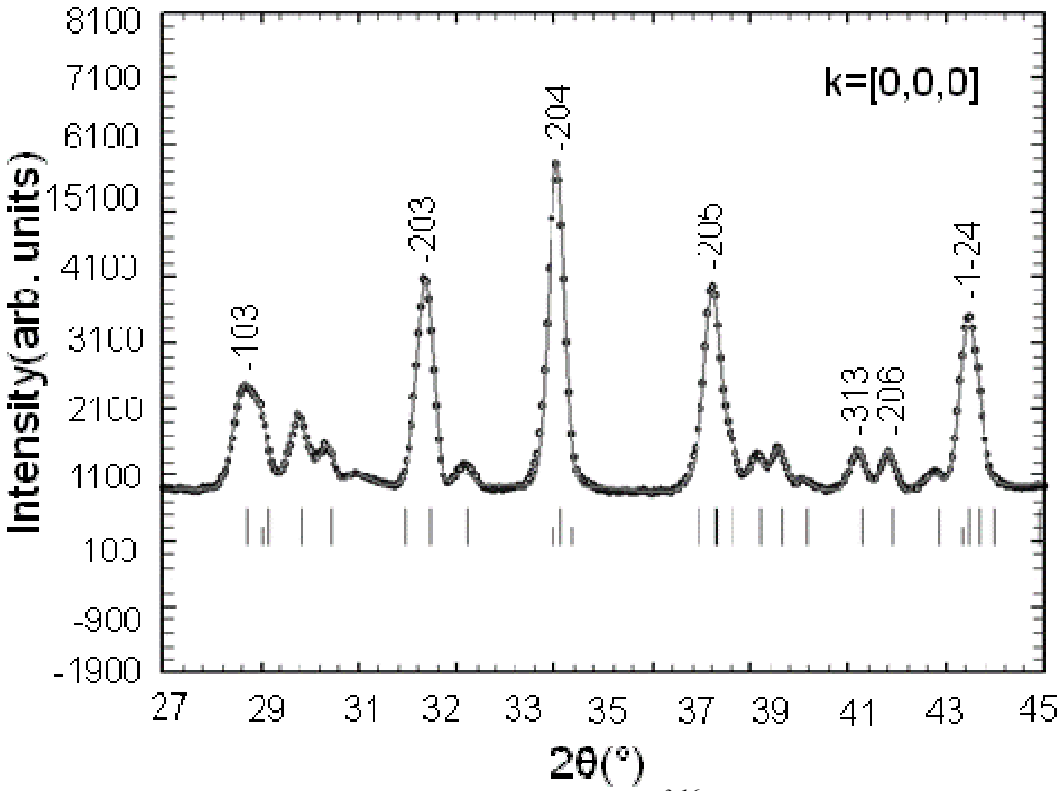

Figure S3g: *The magnetic peaks for 6H-$Ba_{0.8}Sr_{0.2}Fe^{+3.16}F_{0.2}O_{2.48}$ at room temperature, data colected with 3T2 difractometer (λ = 1.2254 Å, Bragg R-factor: 5.86%; Rf-factor= 5.88%; R-mag=5.67%).*

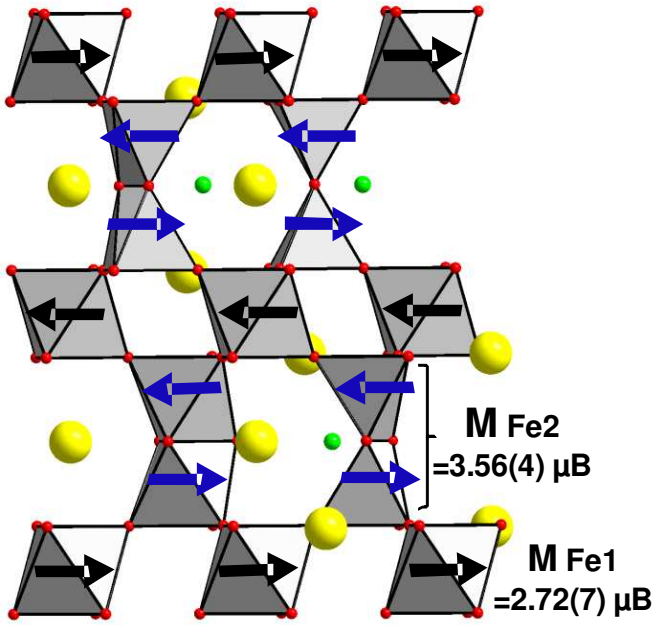

Figure S3h: *Magnetic structure for 6H-$Ba_{0.8}Sr_{0.2}Fe^{+3.16}F_{0.2}O_{2.48}$ at 299K data collected with the 3T2 diffractometer (λ = 1.2254 Å, Bragg R-factor: 5.86%; Rf-factor= 5.88%; R mag=5.67%).*

S4. Magnetic measurements

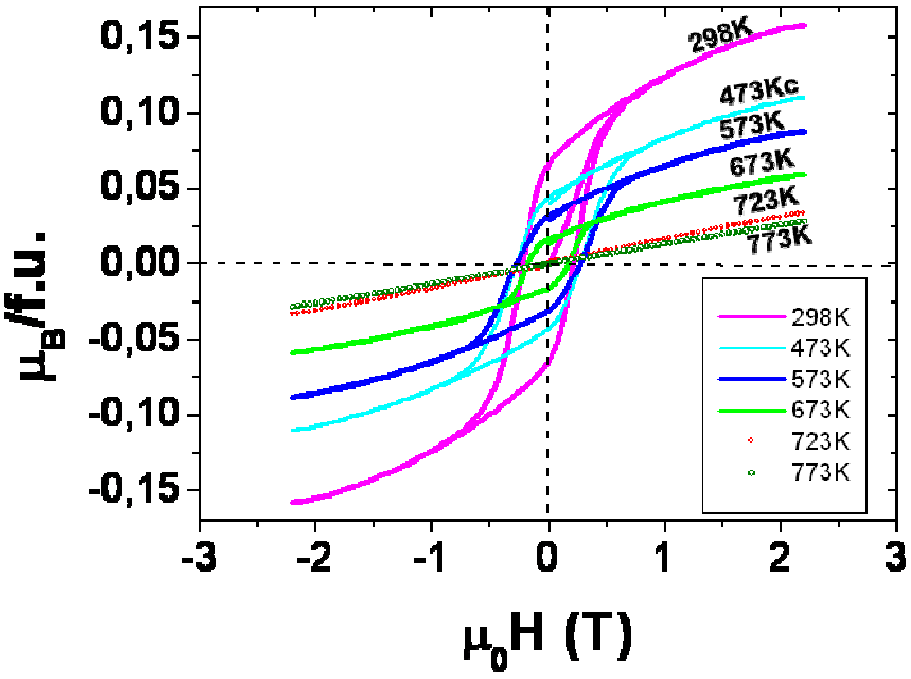

Figure S4a: *Variation of hysteresis loop for 15R-FHP* $BaFeF_{0.2}O_{2.42}$ *function of temperature between 298K and 773K.It shows the existence of weak moment below* T_N.

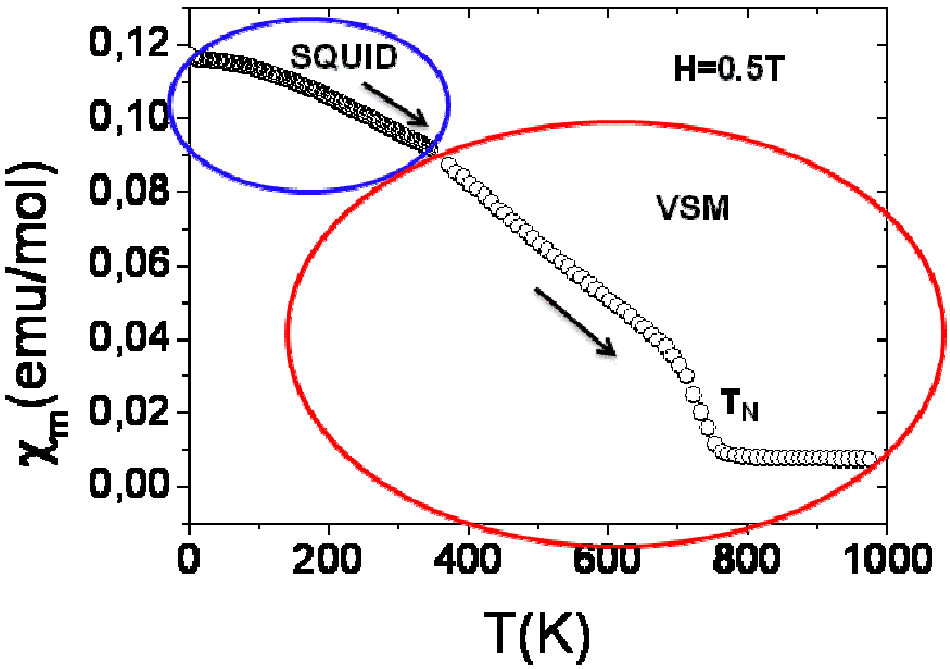

Figure S4b: *Temperature dependence of the molar susceptibility measured in an applied field of 5000 Oe in the full available temperature range.*

Table S4c: Values of ordering temperature, Curie-Weiss temperature and effective magnetic moment for the fluorinated iron compounds depending on the flowing atmosphere. The values have been extracted from data upon heating.

Compound	Atmosphere	T_N (K)	θ_{Cw} (K)	μ_{eff} (μB /Fe)
15R-FHP $BaFeF_{0.2}O_{3-y}$	air	700	-639	4.70
	nitrogen	680	-470	4.42
6H-FHP $Ba_{0.8}Sr_{0.2}FeF_{0.2}O_{3-y}$	air	730	-1711	5.65
	nitrogen	710	-1357	5.25

S5: Ordering temperature in other compounds of the literature

Table S5a: Different values of ordering temperature for the iron compounds

	Compounds	Neel/ Curie-Weiss θ temperature (K)	References
Basic compound	**Fe**	T_C=1043	"Encyclopedia of Physics", vol.XVIII/2, Ferromagnetism,Springer-Verlag, Berlin, **1966**, 4.
	Fe_2O_3	T_N=950	J.E Greedon "*Magnetic oxides* in Encyclopedia of Inorganic chemistry", Ed. R. Bruce King, John Wiley & Sons, **1994**.
	Fe_3O_4	T_C =858	"Encyclopedia of Physics", vol.XVIII/2, Ferromagnetism,Springer-Verlag, Berlin **1966**, 97
	FeO	T_C =570 T_N = 298	"Encyclopedia of Physics", vol.XVIII/2, Ferromagnetism,Springer-Verlag, Berlin **1966**, 100.
Hexagonal perovskite	**15R-$SrMn_{0.9}Fe_{0.1}O_{3-\delta}$**	T_N=220	Cussen, E. J.; Sloan, J.; Vente, Battle, P. D.; Gibb, T. C. *Inorg. Chem.* **1998**, *37*, 6071–6077.
	15R-$BaIr_{0.3}Fe_{0.7}O_{2.949(7)}$ **6H-$BaIr_{0.2}Fe_{0.8}O_{2.932(5)}$**	T_N=200 T_N=220	Jordan, N. A.; Battle, P. D.; Sloan, J.; Manuel, P.; Kilcoyne, S. *J. Mater. Chem.* **2003**, *13*, 2617–2625.
	6H-$BaFeO_{3-\delta}$	T_N=130	Mori, K.; Kamiyama, T.; Kobayashi, H.; Otomo, T.; Nishiyama, K.; Sugiyama, M.; Itoh, K.; Fukunaga, T.; Ikeda, S. *J. Appl. Cryst.* **2007**, 40, 501–505.
	12H-$BaFeO_{3-\delta}$	T_N=172	Takeda**,** Y**.;** Shimada**,** M.; Kanamaru**,** F.; Koizumi**,** M**.;** Yamamoto**,** N. *Mater. Res. Bull.* **1974**, 4, 537 – 543.

	$BaFeO_{2.95}$	T_N=178	Gil de Muro, I.; Insausti, M. ; Lezama, L. ; Rojo, T. *J. Solid State Chem.*, **2005**, *178*, 1712.
Derivate 3C perovskite	**$LaFeO_3$**	T_N=740	Seo, J. W.; Fullerton, E. E.; Nolting, F.; Scholl, A.; Fompeyrine, J.; Locquet, J.-P. *J. Phys. Condens. Matter.* **2008**, 20**,** 264014.
	$SrFeO_2$	T_N=473	Tsujimoto, Y.; Tassel, C.; Hayashi, N.; Watanabe, T.; Kageyama, H.; Yoshimura, K.; Takano, M.; Ceretti, M.; Ritter, C.; Paulus, W. *Nature* **2007**, *450*, 1062–1065.
	$SmFeO_3$	$T_N \backsimeq 623$	Iglesias, M.; Rodrıgueza, A.; Blaha, P.; Pardo, V.; Baldomir, D.; Pereiro, M.; Botana, J.; Arias, J.E.; Schwarz, K. *J. Magn. Mang. Mater.* **2005**,290, 396–399.
	$YbFeO_3$ **$YFeO_3$**	T_N=630 T_N=645	Pinto**,** H.; Shachar**,** G.; Shaked, H. *Solid State Communications* **1970**, 8, 597 – 599.
	PbFeFO2	T_N>500	Inaguma, Y.; Greneche, J.-M.; Crosnier-Lopez, M.-P.; Katsumata, T.; Calage, Y.; Fourquet, J.-L. *Chem. Mater.* **2005***,*17, 1386 -1390
	$BaFeFO_2$	T_N=645	Heap, R.; Slater, P. R.; Berry, F. J.; Helgason, O.; Wright, A. J. *Solid State Commun.* **2007**, *141*, 467–470.
	$SrFeO_2F$	T_N=685	Berry, F. J.; Heap, R.; Helgason, Ö.; Moore, E. A.; Shim, S.; Slater P. R.; Thomas, M. F. *J. Phys. Condens. Matter* **2008**, 20, 215207
Perovskite related structure	**Sr_2Fe_2O5**	T_N=692	Schmidt, M.; Campbell*,* S. J. *J. Solid State Chem.* **2001**, 156, 292 – 304.
	Ca_2Fe_2O5	T_N=720	Berastegui, P.; Eriksson, S.-G.; Hull, S. *Mater. Res. Bull.* **1999**, 34, 303–314.
	$Pb_{1.08}Ba_{0.92}Fe_2O_5$	$T_N \backsimeq 625$	Nikolaev, I. V.; D'Hondt, H.; Abakumov, A. M.; Hadermann, J.; Balagurov, A. M.;. Bobrikov, I. A; Sheptyakov, D. V.; Pomjakushin, V. Yu.; Pokholok, K. V.; Filimonov, D. S. Tendeloo, G. V.; Antipov, E. V. *Physical Review B* **2008 ,** 78, 24426
	$YBa_2Fe_3O_8$	T_N=660	Karen, P.; Suard, E.; Fauth, F. *Inorg. Chem.* **2005**, 44, 8170–8172**.**
	$LaCa_2Fe_3O_8$	$T_N \backsimeq 735$	Hudspeth, J. M.; Goossens, D. J.; Studer, A. J.; Withers, R. L.; Noren, L. *J. Phys. Condens. Matter* **21**, 124206 (2009).

	$Ba_{1.6}Ca_{2.3}Y_{1.1}Fe_5O_{13}$	T_N =750	Demont, A.; Dyer, M. S.; Sayers, R.; Thomas, M. F.; Tsiamtsouri, M.; Niu, H. N.; Darling, G. R.; Daoud-Aladine, A.; Claridge, J. B.; Rosseinsky, M. J. *Chem. Mater.* **2010**, 22, 6598–6615.
Other structure	$BaSrFe_4O_8$	T_N=690	Abbas, Y.; Mostafa, F.; Fayek, M. *Acta.Cryst. B* **1983**, 39, 1-4.
	$BaCaFe_4O_8$	T_N=685	Abbas, Y.; Mostafa, F.; Fayek, M. *J. Phys. Chem. Solids* **1982**,43, 973-975.
	$Ba_2Fe_6O_{11}$	T_N=488	Asti, G.; Carbucicchio, M. ; Deriu, A. ; Lucchini, E. ; Sloccari, G. *Mater. Res. Bull.* **1978**, 13, 153 – 158.
	$BaFe_{12}O_{19}$	T_C=726	Wang, J.; Chen, Q.; Chea, S. *J. Magn. Magn. Mater.* **2004**, 280, 281–286.

S6: Thermal behaviour of 6H-oxide-$BaFeO_{3-\delta}$

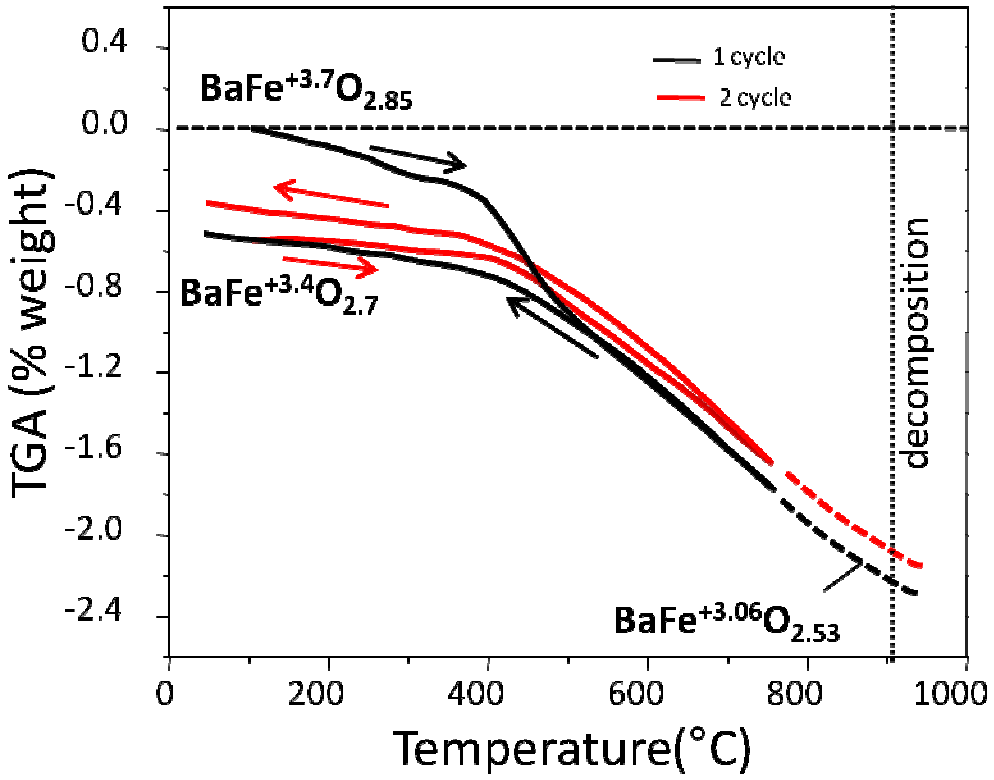

Figure S6: *Thermal gravimetric analysis under flowing air, under two subsequent heating/cooling cycles from 6H-BaFeO~2.85*